12-2014

Synthesis and Characterization of Ln[hfac]x and Ln[fod]x Complexes for Thermochromatographic Separations

Matthew L. Marsh

University of Tennessee - Knoxville, mmarsh6@vols.utk.edu

Synthesis and Characterization of Ln[hfac]$_x$ and Ln[fod]$_x$ Complexes for Thermochromatographic Separations

by

Matthew Marsh

Fall 2014

Acknowledgements

Table of Contents

List of Tables and Figures

iv

Abstract

Solution phase separations are a fundamental process for performing radiochemical analysis. However, traditional solution-based separations are generally slow; therefore, the need for more rapid separation techniques is essential. This work involves the exploitation of gas-phase chemistry for the isolation of fission and activation products in the immediate aftermath of a nuclear explosion. Gas thermochromatographic separations of the rare earth elements followed by subsequent detection by mass spectrometry will be discussed. The rare-earths can be readily volatilized with either 1,1,1,5,5,5-hexafluoroacetylacetonate (hfac) or 6,6,7,7,8,8,8-heptafluoro-2,2-dimethyl-3,5-octanedione (hfod) at temperatures above 150°C. The synthesis and structural characterization of these complexes were found to vary slightly by the assortment of ligands, hydration degree, and impurities with potentially large implications toward the specific thermochromatographic elution data. Under the parameters used, better separations of a triple rare-earth sample were found with the use of the hfac ligand as opposed to hfod. This method offers the advantage of rapid, carrier-free separations, in addition to providing elemental and isotopic composition information regarding a given sample in support of nuclear forensics analysis. Furthermore, this work also supports the growing need for rapid separation and analysis of short-lived isotopes currently being used in the radiopharmaceutical industry, nuclear medicine, and research efforts in the super heavy element discovery.

I.   Introduction

The ability to separate fission and activation products that are formed in post-detonation events in the fallout of a nuclear device is very important to the nuclear forensics community. Currently, the ability to determine the fission and activation products requires lengthy sample preparation times and further require the use of gamma-ray spectroscopy or thermal ionization mass spectrometry (TIMS) to determine the identity and concentration of the elemental components. The use of TIMS and gamma-ray spectroscopy is also used to determine the isotopic composition (e.g. isotopic ratios) of the obtained samples. It is therefore of interest to develop sample preparation methods that can reduce the time required to perform the sample analysis, while retaining equivalent accuracy and precision to the established methods.

In order to perform this work, it was decided to employ thermochromatographic techniques followed by subsequent detection. Organometallic compounds showing high volatility have been an area of research interest for many years. One potential application for this includes chemical vapor deposition (CVD), but the differing volatilities of similar compounds make gas-phase separation a potentially fruitful area.[1] One area that has shown promise is the use of β-diketonates as the ligand group on rare-earth metals to volatilize the rare earth.[2] The volatility of the complex can be manipulated by changing the gamma carbon on the β-diketonate. This substitutional flexibility provides numerous possibilities for compounds. A simple modification to the γ-carbon can shift the melting point a few degrees,[3] while more complex substitutions can shift the melting point more than 50°C.[4]

Each of the β-diketonates used as ligands has similar synthesis methodology; however, the specific materials used in each synthesis are unique, with different yields, hydrations, and

1

unpurified sample characteristics.[1, 4, 5] Even for the same compound separate methods exist for synthesis and purification.[4, 6, 7]

This work evaluated the synthesis method used by Berg and Acosta[4] to synthesize hexafluoroacetylacetone (hfac) complexes for the entire lanthanide series (excepting promethium and cerium) and to characterize the resulting compounds in order to establish the methodology required to synthesize these compounds for thermochromatographic separations.[8] It also evaluated a similar synthesis method performed by Springer et al[5] to synthesize 6,6,7,7,8,8,8-heptafluoro-2,2-dimethyl-3,5-octanedione (fod) complexes for thermochromatographic separations and compared the separation data between these two ligands.

II.   Synthesis

A. *Ln[hfac]$_x$*

Compounds for La-Lu were synthesized similarly. A typical procedure is described for lanthanum. The La_2O_3 was combined with hot, concentrated HCl (Fisher) to yield the chloride salt in an acid solution. The solution was allowed to cool and was stored. Since hexafluoroacetylacetone (hfac) is a weak acid, low pH has an adverse effect on its reaction with the $LaCl_3$. A 500 μL sample of the solution was taken and evaporated of its solvent, leaving pure $LaCl_3$. This $LaCl_3$ was redissolved in 500 μL of water.

Hexafluoroacetylacetone (Acros) was first obtained and combined with equimolar amounts of concentrated NH_4OH (Fisher). The two liquids reacted vigorously, producing a white solid (NH_4[hfac]) that was stirred to fully react the reagents. The solid was then placed in a desiccator for storage.

The NH_4[hfac] was dissolved in 4-5 mL of diethyl ether (Fisher) to which the aqueous $LaCl_3$ was added in a molar ratio of 1 La : 4 ligand. The mixture was shaken vigorously for 30

seconds, and then set for 5 minutes, repeating 3 times. At the conclusion of the last separation, the organic phase was drawn off and placed in a vacuum desiccator to dry the sample and remove the ether. A solid residue remained after 24 hours of drying, and this resulted in La[hfac]$_x$. After desiccation, the remaining residue was a white powder. This synthesis method was used for the Gd complex (Gd[hfac]$_x$) and for Lu (Lu[hfac]$_x$), principally, as well as for the other rare-earth elements (excepting Ce and Pm).

B. *Ln[fod]$_x$*

Synthesis of the fod complexes utilized a precipitation reaction. Dried ammonium fod (NH$_4$[fod]) synthesized from 6,6,7,7,8,8,8-heptafluoro-2,2-dimethyl-3,5-octanedione (Acros) and equimolar amounts of concentrated NH$_4$OH (Fisher) was dissolved in 4-5 mL of diethyl ether. One millimole (mmol) of rare-earth chloride was dissolved into 50 mL of water and added to the 4 mmol of dissolved NH$_4$[fod]. The solution was allowed to rest for at least 3 minutes, and the solution was centrifuged and filtered using a Büchner . The resultant material was dried under vacuum. Synthesis included all rare-earth elements excluding Ce and Pm.

III.   Characterization

A. *Ln[hfac]$_x$*

i.) SC-XRD. (SC-XRD to determine crystal structure was only achieved for Gd)

Data was collected on a Bruker SMART APEXII three circle diffractometer equipped with a CCD area detector and operated at 1,800 W power (45 kV, 40 mA) to generate Mo Kα radiation ($\lambda = 0.71073$ Å). The incident X-ray beam was focused and monochromated using Bruker Excalibur focusing optics. Single crystals were mounted on nylon CryoLoops (Hampton Research) with Paratone-N (Hampton Research) and frozen at -100 ℃ and -173 ℃, respectively. Initial scans of each specimen were taken to obtain preliminary

unit cell parameters and to assess the mosaicity (i.e. breadth of spots between frames) of the crystal to select the required frame width for data collection. For all cases frame widths of 0.5° were judged to be appropriate and full hemispheres of data were collected using the Bruker APEX2 software suite to carry out overlapping φ and ω scans at detector setting of $2\theta = 28^{o}$.

Following data collection, reflections were sampled from all regions of the Ewald sphere to re-determine unit cell parameters for data integration. Following exhaustive review of collected frames the resolution of the dataset was judged, and, if necessary, regions of the frames where no coherent scattering was observed were removed from consideration for data integration using the Bruker SAINTplus program. Data was integrated using a narrow frame algorithm and was subsequently corrected for absorption. Absorption corrections were performed for both samples using the SADABS program. Space group determination and tests for merohedral twinning were carried out using XPREP. The highest possible space group was chosen.

The final model was refined anisotropically (with the exception of H atoms). Hydrogen atoms were not placed on solvent molecules due to disorder. The structure was examined using the Addsym subroutine of PLATON4 to assure that no additional symmetry could be applied to the models. The structure arrived at is shown in Figure 1.
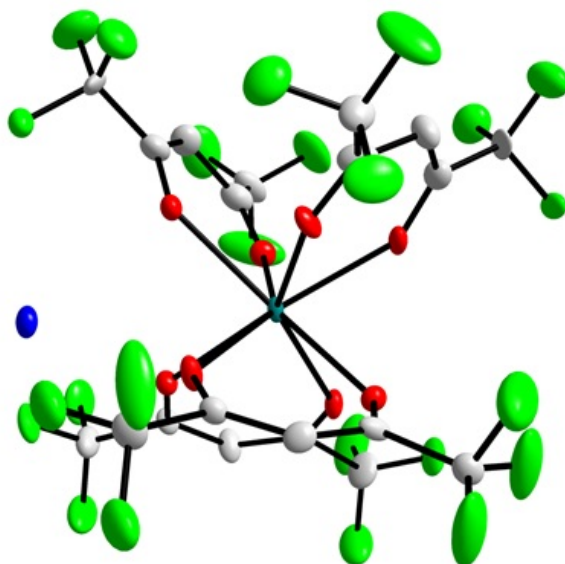
Figure 1- Crystal Structure of $NH_3^+(Gd[hfac]_4^-)$. The nitrogen (blue), fluorine (green), carbon (white), oxygen (white), and gadolinium (grey) are shown, while hydrogen atoms are omitted for clarity.

The resulting crystal structure has a single gadolinium atom bound to 8 oxygen atoms forming a trigonal anti-pyramidal geometry. The lone NH_4^+ cation likely forms a hydrogen bond to the trifluoromethane groups of the ligand.

ii.) Elemental Analysis and FT-IR Spectroscopy.

Elemental analysis and IR data were produced for all the rare-earths. Elemental analysis was performed by Atlantic Microlab in Norcross, GA. Infrared spectra were recorded using a Perkin Elmer FT-attenuated total reflectance – infrared spectrometer (FT-ATR-IR) spectrum 100 instrument in the range from 620-4000 cm^{-1}. The data is laid out succinctly below for La, Gd, and Lu (Tables 1-3) while the other rare-earth metals are displayed in Appendix 1 (yield and elemental analysis). Additional IR spectra will be discussed in a later section.

Table 1- Elemental and FT-IR analsysis of La[hfac]$_x$

Compound	La: 63.97-66.31% yield					
Elemental Analysis	Element	Theory	Found	% Error		
	C	23.55	24.7	5%		
	H	1.28	1.31	2%		
	N	2.75	2.65	4%		
	F	44.69	43.41	3%		
IR (ATR cm^{-1})	Shift	Peak	Shift	Peak	Shift	Peak
	3332	br	1203	s	908	m
	1645	w	1187	m	864	w
	1615	w	1175	m	822	w
	1563	w	1130	br, s	806	w
	1537	w	1095	sh	784	w
	1458	m	986	m	737	m
	1270	m	968	m	659	m

Table 2- Elemental and FT-IR Analysis of Gd[hfac]$_x$

Compound	Gd: 57.89-59.97% yield. (58.91%)					
Elemental Analysis	Element	Theory	Found	% Error		
	C	23.54	24.35	3%		
	H	0.99	0.96	3%		
	N	2.06	2.195	6%		
	F	44.68	42.74	5%		
IR (ATR cm^{-1})	Shift	Peak	Shift	Peak	Shift	Peak
	3127	br	1472	w	804	s
	3040	br	1405	m	768	w
	1645	s	1349	w	752	w
	1611	w	1253	s	744	s
	1563	w	1201	s	661	s
	1537	m	1136	s		
	1502	w	1096	s		

When calculating the theoretical elemental compositions reported, the values were for 4

coordinating ligands, since, as the results from Figure 1 have illustrated, there is some

speculative evidence that the molar ratio [M] of ligand added corresponds to the same

statistically favored thermodynamic product. In this case, SC-XRD for $Gd[hfac]_x$ produced

$NH_3^+(Gd[hfac]_4^-)$. Nominally observed analogs by Sievers et al.[9] for the triethylammonium and

tetraethylammonium tetrakis complexes, though understudied, provides other evidence for this

effect in the literature. Theoretical compositions also seek to minimize error due to $NH_4[hfac]$

impurities as well as hydration effects. For example, as one progresses from La → Gd → Lu, the

general contraction of ion size has a lesser degree of ammonium and hydration effects that are

able to coordinate. As a result, it might be expected to see higher yields across the series.

However, this was not the case.

Percent yields are given as a range in the table, the minimum representing pure SC-XRD

data and a maximum representing the general observation of 2 outer-coordinating bodies (1

ammonium plus 1 water). In reality, it is something between this. Finally, parenthetical yields

attempt to remove $NH_4[hfac]$ impurities from the result. The actual elemental analysis that was

performed by Atlantic Microlabs and by ICP-TOF-MS results from our laboratory was in good

agreement with the theoretical data.

In sum, the elemental analysis and SC-XRD results calculated a complex that has more

than 3 hfac ligands, as additionally cited by both Binnemans[2] and Berg and Acosta[4]. As seen in

Table 4, the results support an overall coordination number of 8 for each complex. This could

involve 4 bidentate hfac ligands split equally around a three-dimensional axis (which would

agree with the one SC-XRD result). However, as will be seen with the NMR, this only happens

to be one possibility. For a state of monohydration, one H_2O molecule would coordinate in the

outer-coordination sphere to give the molecule its respective hydration. Finally, ammonium

counter-ions would exist to give the excess ligand stability in diethyl ether.

Table 3- Lu[hfac]$_x$

Compound	Lu: 52.38-54.23% yield. (53.76%)					
Elemental Analysis	Element	Theory	Found	% Error		
	C	23.44	23.62	1%		
	H	0.79	0.78	1%		
	N	1.71	1.63	5%		
	F	44.5	42.09	6%		
IR (ATR cm^{-1})	Shift	Peak	Shift	Peak	Shift	Peak
	3253	br	1356	w	966	m
	3049	w	1337	w	907	m
	1652	w	1271	m	821	m
	1562	w	1204	s	738	m
	1536	w	1177	s	660	s
	1456	m	1115	s		
	1409	w	985	m		

Table 4-Translation of Elemental Analysis to Ligand Number and Coordination

Compound	Number of hfac ligands	# of H$_2$O or NH$_4^+$	Overall Coordination #
La	4	1 NH$_4^+$ and 1 H$_2$O	8
Gd	4	0.5 NH$_4^+$ and 0.5 H$_2$O	8
Lu	4	0.25 NH$_4^+$	8

iii.) Computational Analysis. Based on discussions with computational chemist collaborators,

the computational product of these compounds can include from three to as many as six

coordinating ligands, with some combination between 3-4 bidentate ligands and 2-3 monodentate

ligands completing a coordination of 8. A higher ligand concentration may drive this sort of

crowded product, if it is true. The Gibbs free energy for the six-ligand computational product

was derived from density functional theory and the B3LYP functional. An example for La and Lu is shown below:

$$LnR_3(HR)_{n\ (g)}\ for\ Ln = La,\ Gd,\ Lu;\ HR = \text{Hfac};\ n = 3\ for\ La,\ and\ Gd,\ and\ 2\ for\ Lu$$

$$La^{3+}{}_{(g)} + 3\ hfac^-{}_{(g)} + 3\ hfac_{(g)} \rightarrow LaR_3(HR)_{3\ (g)} \quad Rxn.\ I$$

$$Lu^{3+}{}_{(g)} + 3\ hfac^-{}_{(g)} + 2\ hfac_{(g)} \rightarrow LuR_3(HR)_{2\ (g)} \quad Rxn.\ II$$
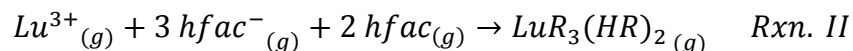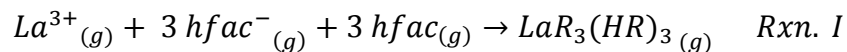
$$\Delta(\Delta G)_{Rxn\ II-Rxn\ I} = -110.39\ kcal$$

This example demonstrates the computational trend across the series that ΔG becomes more negative and the ligand association becomes most favored for Lu, albeit slight differences in coordination.

A theoretical image for La that corresponds to the computational and elemental analysis results is presented in Figure 2. This is also analogous to the SC-XRD data for Gd. Table 5 shows a comparison of the bond lengths between the gadolinium atom to the oxygen atoms in the coordination shell, as well as the ammonium. The bond lengths of the calculated structure were in good agreement with the structure from the x-ray crystallographic data. It is important to note that the optimized geometry (calculated) is in the gas phase, while the x-ray crystallographic structure is a crystal (in the solid phase). Therefore, some differences in the structure are expected.
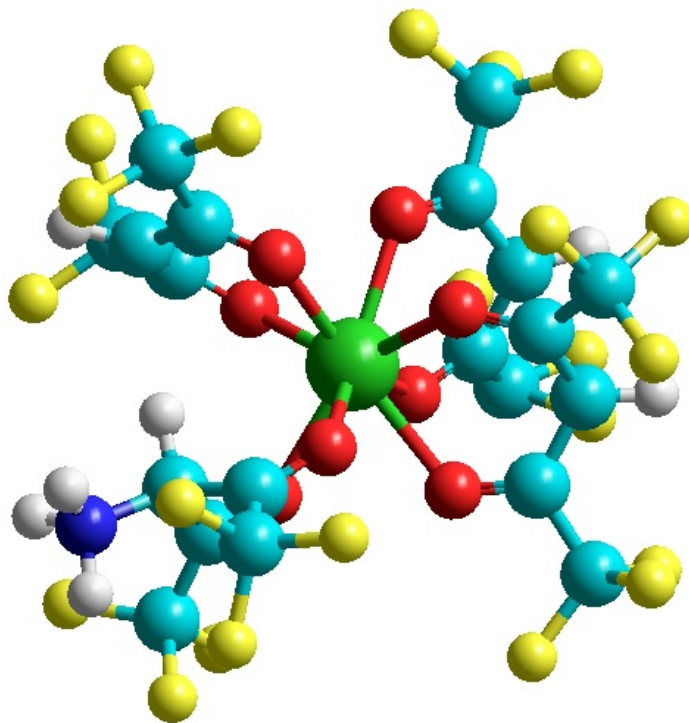
Figure 2-Optimized Geometry for $NH_3^+(La[hfac]_4^-)$. The lanthanum (green), the oxygen (red), carbon (grey), fluorine (yellow), nitrogen (blue), and hydrogen (white).

Atom 1	Atom 2	Distance (Å)		
		Calculated	Experimental	Diff
Gd	O1	2.448	2.371	0.077
Gd	O2	2.390	2.350	0.040
Gd	O3	2.343	2.377	-0.034
Gd	O4	2.529	2.413	0.116
Gd	O5	2.409	2.389	0.020
Gd	O6	2.405	2.394	0.011
Gd	O7	2.384	2.395	-0.011
Gd	O8	2.301	2.318	-0.017
Gd	N	3.930	3.936	-0.006
N	H5	1.049	not available	-
N	H6	1.025	not available	-
N	H7	1.047	not available	-

Table 5-Comparison of calculated bond lengths and experimental results.

iv.) Melting point.

The melting point of the powders was determined using a Mettler Toledo MP50 Melting Point System. Four samples were measured per batch. The samples, excepting the $NH_4[hfac]$,

were first heated in a sample oven to between 90-100°C to remove any trace contaminants (particularly trace NH_4[hfac]) to prepare them for melting point analysis. Table 6 presents the averaged melting points.

Table 6-Melting Points for Ln[hfac]$_x$ Compounds

Compounds	Range (°C)	Compounds	Range (°C)
NH_4	86-91	Tb	194-203
La	142-146	Dy	203-211
Pr	179-184	Ho	220-223
Nd	178-185	Er	221-224
Sm	189-195	Tm	202-212
Eu	178-188	Yb	213-218
Gd	181-191	Lu	212-219

Previous reports for representative compounds, as noted by Binnemans[2], have given the melting points for La to be 143-146 °C, for Gd to be 170-173°C, and for Lu to be 222-223°C. However, the compounds presented by Berg[4] and Binnemans[2] were the dihydrate compound motif. Figure 3 illustrates the trend between the contraction of atomic radii and higher melting point. The atomic radii used are Shannon-Prewitt radii[10,11] for the eight-coordinate lanthanide complexes. This data provides a better substitute for molecular weight data when assessing the phase-transition equilibria across the series, and, as one might assume, fits the data better on a directly comparable basis.
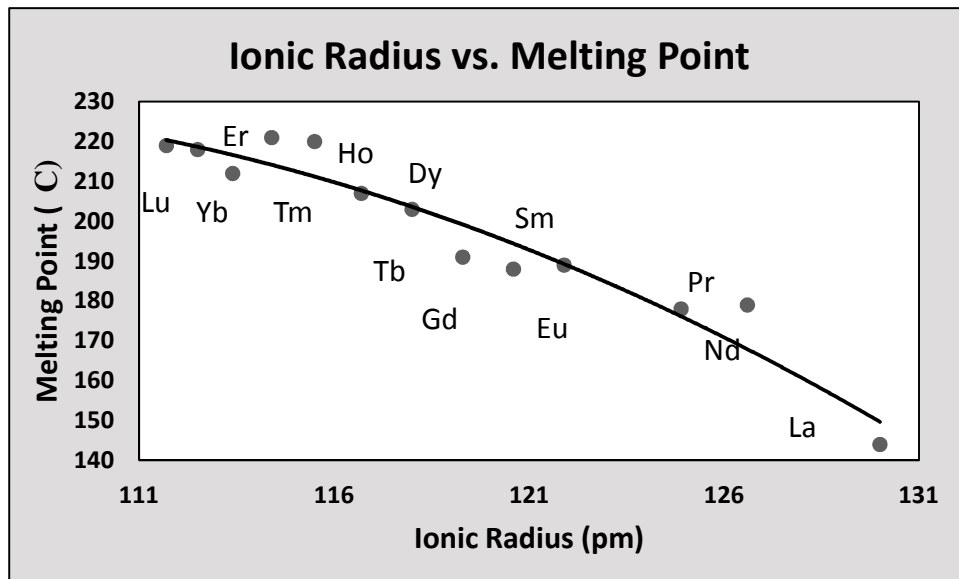
Figure 3-Distribution of Melting Points as a function of Atomic Radii

v.) Infrared (IR) Spectroscopy. The FT-IR measurements were carried out on a Nicolet iS10 ATR-IR (attenuated total reflectance) instrument, and were analyzed from 4500 to 550 cm^{-1}.

Once again, only La, Gd, and Lu are shown in Table 7, but are representative of the entire series. Appendix 2 includes an expanded table for all the rare-earths analyzed. The IR peaks for La[hfac]$_x$ were in agreement with the data from Richards et al. and Condorelli et al, and the functional groups were assigned based on those values. The work by Richards evaluated the trihydrate, while in Condorelli hydrate-free gas phase IR measurements were performed in addition to n-hydrated La[hfac]$_x$.[12, 13] The measurement data obtained contained four key data points signifying a metal-coordinated ligand.[13]

The major peaks from both of these papers were all identified and are listed in Table 7. Similar peaks were found for the NH$_4$, Gd, and Lu as well. Table 7 presents the peak value and its associated functional group for each of the four compounds.

12

Excellent correlation is found between the wavenumbers of the compounds even from opposite ends of the lanthanide family, agreeing with previous literature.[12] The $NH_4[hfac]$ compound was lacking two of the metal-ligand wavenumbers which were clearly identified on the other three complexes. The $Gd[hfac]_x$ complex was missing one of the three CF_3 stretching peaks which was unexpected and its cause remains undetermined.

Table 7- IR peaks (cm^{-1}) and functional group assignments for $Ln[hfac]_x$ complexes

NH_4	La	Gd	Lu	Functional Assignment
738	737	744	738	C-CF_3 stretch
799	806	804	821	C-H out of plane bend
1113	1130	1136	1115	C-H in-plane bend
1176	1187		1177	C-F stretch
1203	1203	1202	1204	C-F stretch
1271	1270	1253	1271	C-F stretch
1455	1458	1472	1456	C-H bend, [hfac]-metal coordination
	1537	1537	1536	C-O stretch, C-H bend, [hfac]-metal coordination
	1563	1563	1562	C=C stretch, [hfac]-metal coordination
1656	1645	1645	1652	C-O stretch, [hfac]-metal coordination
3260	3332	3040	3253	O-H stretch

vi.) Nuclear Magnetic Resonance (NMR) Spectroscopy. NMR measurements were carried out on a Varian Inova 500 MHz instrument. The solvent used was 1,4-dioxane$_{(D-99.9\%)}$. Most other solvents are incompatible with the ligand[14]. Table 8 shows the relative shifts of ^{13}C, ^{1}H, and ^{19}F NMR for the ligand (hfac) by itself in the left column while relative shifts for $La[hfac]_x$ are in the right column. Several peaks have complementarity to the literature reference[14].

For the ^{13}C NMR, peaks (in ppm) are documented as follows: 93.5 corresponds to the α-carbon, 117 to the γ-carbon, and 173.3 to the β-carbon. The peak at 93.5 showed a pentet that is

split both by the hydrogens and the fluorines. Both the β and γ-carbons were quartets that are split by the fluorine groups. As can be noted, there is no data for the La complex due an issue with the C-probe. This data will be determined in the future.

For the ^{1}H NMR, the ligand by itself shows a strong peak at 6.43 ppm corresponding to the hydrogens on the α-carbon. La[hfac]$_x$ shows this peak at 6.60 ppm. The peaks at 2.24 ppm and 2.81 ppm are peaks for ammonium hydrogens that depend on their relative chemical environment. Recall that La has a coordination number of 8-9 with hfac, and that it can either divide this between 4 bidentate ligands or with 3 bidentate and 3 monodentate ligands. Ultimately, the intensity of the shifts should reflect the probability of association with bidentate or monodentate ligands. For example, ammonium cations associating with monodentate ligands should be shifted at 2.81 ppm. This makes sense with respect to the shift, as ammonium coordinated to a monodentate site should experience a stronger deshielding effect from an electronegative oxygen with free electrons as opposed to a bound oxygen.

The HMBC in Figure 4 shows a comparison of the ligand to that of the ligand after treatment with ammonium hydroxide. The hydrogen peak at 6.45 ppm is on the same chain as that of the other 3 carbon peaks and is directly linked to the carbon at 93.4 ppm. After treatment, the hydrogen shifts downfield to a position at 5.7 ppm, but remains bonded to the previous 3 carbons. Due to solubility differences between the two substances, the NH$_4$[hfac] is much weaker, but all of the carbon peaks remain at the original shift positions.

For the ^{19}F NMR, the ligand by itself showed a strong peak at -77.75 ppm. This corresponded to -77.26 ppm in the La[hfac]$_x$ complex. Once again, depending on the range of monodentate or bidentate formations from the ligand, the fluorines are asymmetric and give separate signals. The signal at -87.98 ppm was very strong and this parallels the concept of the

ammonium hydrogens. This signal then represents the fluorines in the bound sites. The signal

intensities at -87.2 ppm and -80.1 ppm were both equivalent, representing the unbound sites.

Fluorines showing a signal at -87.2 ppm represent fluorine atoms closer to the center of the

complex in the unbound sites, while the fluorine atoms showing a signal at -80.1 ppm represent

fluorines farther away from the center of the complex in the unbound sites. Figure 5 shows the

two spectrums for the ^{1}H and ^{19}F NMR.

Table 8-NMR peaks (ppm) for hfac and La[hfac]$_x$

Nuclei	hfac	La[hfac]x
C	δ: 93.5 (m), 117 (q), 173.3 (q)	
H	δ: 6.43 (s)	δ: 2.24 (s), 2.81 (s), 6.60 (s)
F	δ: -77.75	δ: -77.26 (s), -80.1 (s), -87.2 (s), -87.98 (s)
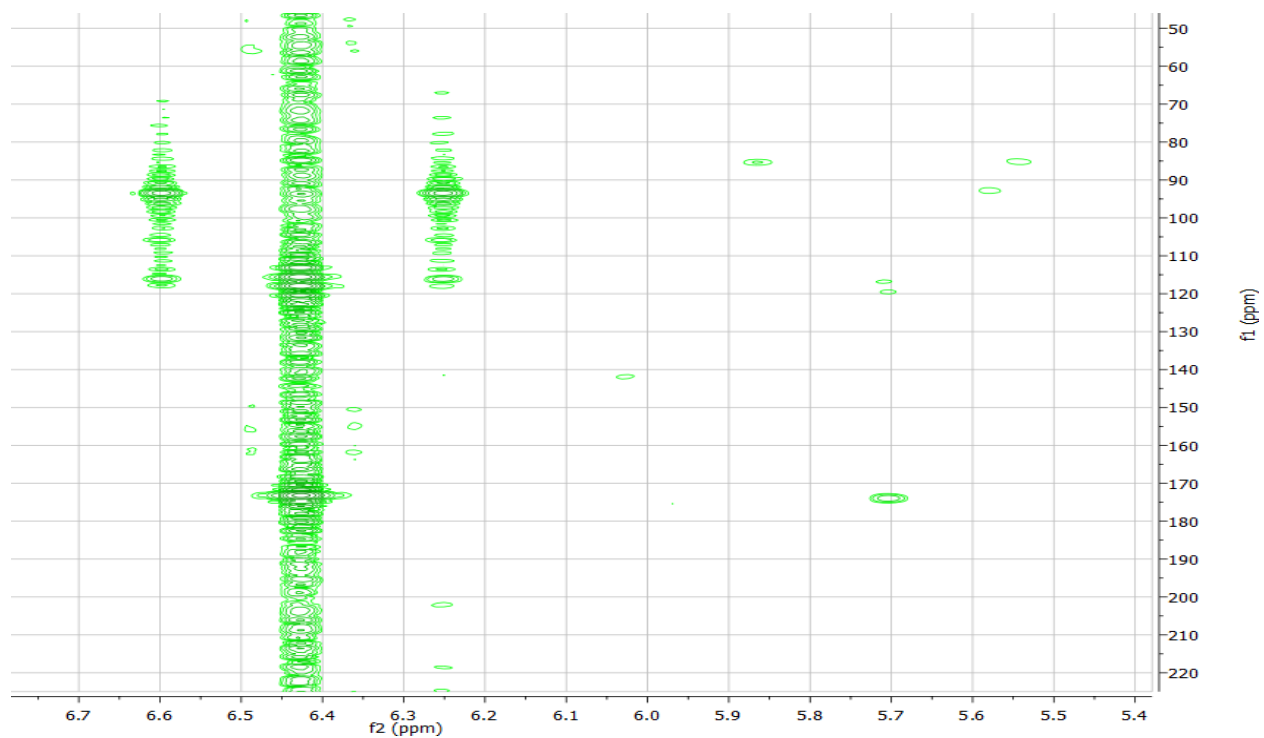
Figure 4-HMBC experiment of both C-13 (y-axis) and H-1 (x-axis)
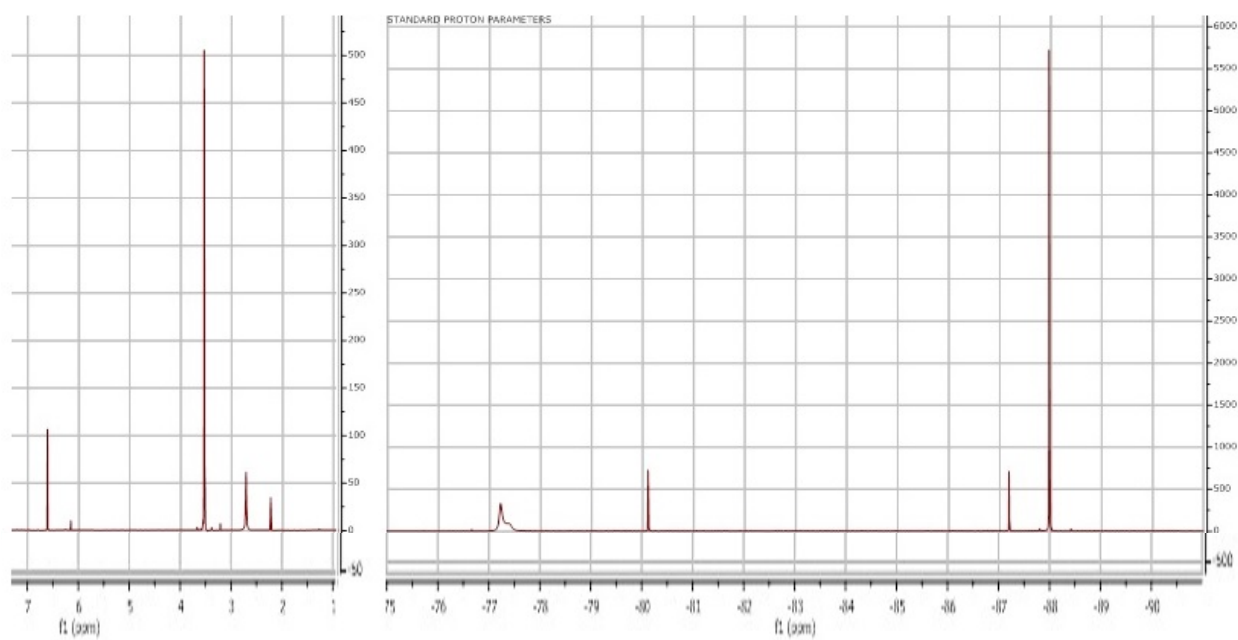
Figure 5-^{1}H-NMR spectrum on the left, ^{19}F-NMR spectrum on the right for La[hfac]$_x$

16

B. *Ln[fod]ₓ*

i.) Elemental Analysis and FT-IR Spectroscopy. All measurements taken used the same

procedures as carried out for the hfac ligand. Data given for La, Gd, and Lu (Tables 9-11) are

laid out succinctly below while the other rare-earths are displayed in Appendix 3.

Table 9- Elemental and FT-IR analysis of La[fod]ₓ

La: 7.79-8.06% yield.					
Element	Theory	Found	% Error		
C	30.46	31.54	3%	Shift	Peak
H	2.9	2.905	0%	1070	m
N	0	0	0%	1020	w
F	33.72	32.73	3%	963	m
Shift	Peak	Shift	Peak	938	w
2974	br	1344	s	909	m
1624	s	1276	w	833	m
1509	s	1220	s	797	m
1458	s	1178	m	755	m
1396	w	1150	s	741	m
1368	w	1117	s	667	m

Compound formulas were determined by minimizing the error between the calculated

values and the data provided by Atlantic Microlab. Errors were generally 1-2%, with values

higher than 4% being occasionally found on N and H. This was attributed to slight residual

impurities of NH_4 remaining within the synthesized complex. Two chemical structures resulted

from the analysis, Ln[fod]₄ and Ln[fod]₃.

The structures for these two complexes are shown in Figures 6 and 7. The four-ligand

complex was found in each of the rare-earths except La. The three-ligand complex was found for

La. For Sm and Yb, the sample was determined to be a mixture of both the three and four ligand

complexes. With the Er and Tb complexes, trace impurities of NH_4[fod] were found within the sample; however, it was undetermined if this fifth ligand was bound to the central atom or not. The formula determination found water present in the sample mixtures. Two water molecules were consistently found throughout the series, irrespective of the compound formula. This can be attributed to the synthesis methodology or adsorption from the atmosphere.

Table 10- Elemental and FT-IR analysis of Gd[fod]$_x$

Gd: 15.83-16.25% yield.					
Element	Theory	Found	% Error		
C	34.56	34.99	1%	Shift	Peak
H	3.34	3.515	5%	1070	m
N	1.01	1.035	2%	1016	w
F	38.27	38.47	1%	964	s
Shift	Peak	Shift	Peak	939	m
2971	br	1350	m	913	w
1627	s	1281	w	833	m
1593	w	1262	w	796	m
1515	s	1203	s	756	m
1471	m	1178	s	735	m
1395	w	1145	s	696	m
1366	w	1116	s	641	w

In the past, only the tris complex has been reported[2, 9]. As was for the case with the thd ligand (dipivaloylmethane), there has been speculation that the fod ligand might be too bulky to form the tetrakis complex[9]. However, it is surprising that of the rare-earth elements across the series, lanthanum was the one found to be in only the tris complex since it has a larger size capability.

Table 11- Elemental and FT-IR analysis of Lu[fod]$_x$

Lu: 57.89-59.97% yield. (58.91%)					
Element	Theory	Found	% Error	Shift	Peak
C	34.13	34.585	1%	1115	s
H	3.29	3.235	2%	1072	m
N	1	1.045	4%	1025	w
F	37.79	38.16	1%	965	m
Shift	Peak	Shift	Peak	939	w
2973	br	1395	w	911	s
1622	s	1367	w	833	m
1585	w	1345	s	793	m
1538	w	1281	w	755	m
1511	s	1223	s	740	m
1467	w	1183	s	689	m
1437	m	1152	s	631	m

Percent yields are once again given as a range in the table, the minimum representing a three or four-ligand anhydrous complex and a maximum representing the general dihydrate complex. The dihydrate is most likely. Parenthetical yields attempt to remove NH_4[hfac] impurities from the result.

As seen in Table 12, the results support an overall coordination of 8 for each complex. For most of the compounds, this would involve 4 bidentate fod ligands split equally around a three-dimensional axis. For the dihydrate state, two H_2O molecules would coordinate in the outer-coordination sphere. As for the case of lanthanum, for example, three bidentate fod ligands surround the central metal ion. Two water molecules in this case would bind to the central metal ion as well. Finally, any assessed ammonium impurities serve to give any excess ligand stability in diethyl ether.

Table 12- Translation of Elemental Analysis to Ligand Number and Coordination

Compound	Number of fod ligands	# of H_2O	Overall Coordination #
La	3	2 H_2O (inner)	8
Gd	4	2 H_2O (outer)	8
Lu	4	2 H_2O (outer)	8
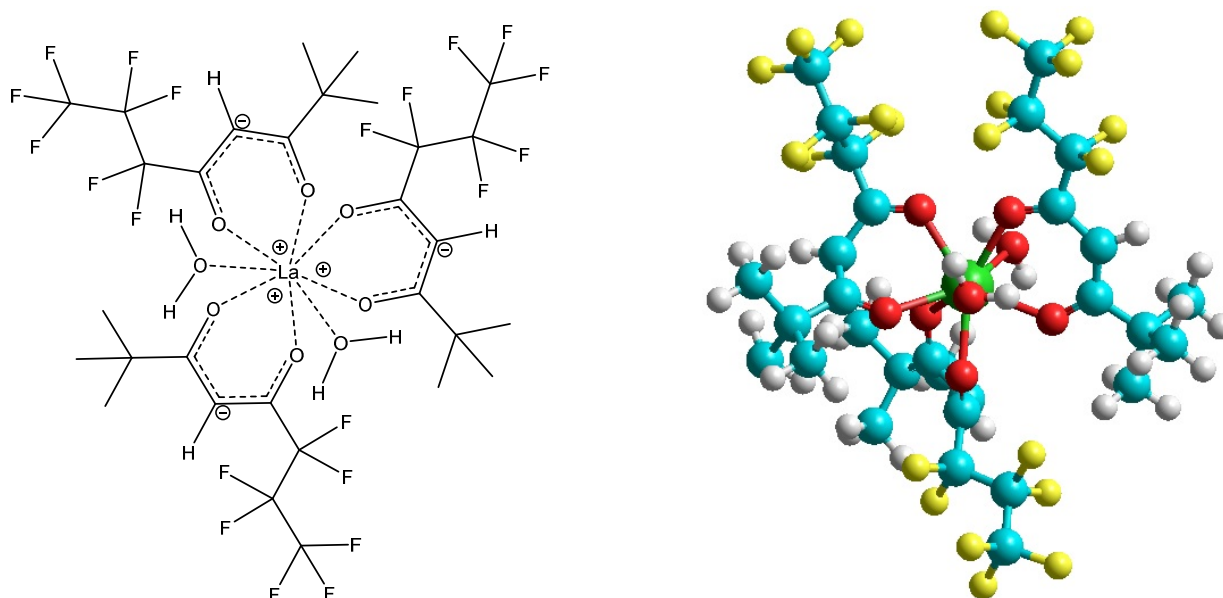
Figure 6- La[fod]$_3$ •2H$_2$O in 2-D (left) and 3-D (right) Representation
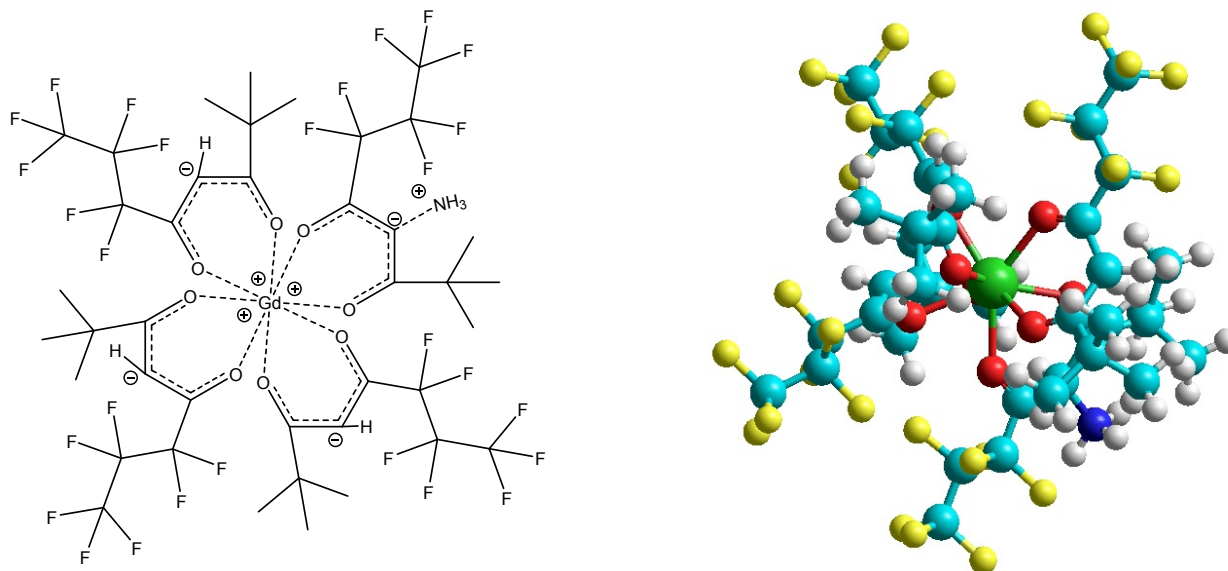
Figure 7- $NH_3^+(Gd[fod]_4^-)$ in 2-D (left) and 3-D (right) Representation

ii.) Melting Point. $Ln[fod]_x$ samples, unlike $Ln[hfac]_x$, did not require preparation before

melting and are presented in Table 13. Previous reports for representative compounds, as noted

by Springer et al.[5], have given the melting points for La to be 215 -230°C (decomposition), for

hydrated Gd to be 60-65°C (anhydrous 203-213°C with decomposition), and for hydrated Lu to

be 111-115°C (anhydrous 118-125°C).

Table 13-Melting Points for $Ln[fod]_x$ Compounds

Compounds	Range (°C)	Compounds	Range (°C)
NH$_4$	<100	Tb	151-152
La	138-146	Dy	136-142
Pr	126-133	Ho	136-141
Nd	116-125	Er	131-136
Sm	119-125	Tm	144-146
Eu	145-150	Yb	134-137
Gd	137-145	Lu	131-136

Figure 8 graphically illustrates the distribution of melting points. Unlike for the case of

$Ln[hfac]_x$, Shannon-Prewitt radii[10,10] for the eight-coordinate lanthanide complexes do not

correlate well and hence do not explain the distribution. While the melting points initially show a decrease for the light-lanthanides, the middle-lanthanides show their own trend as well as the heavy lanthanides. As varied as the melting points become due to slight hydration differences, it is difficult to establish a trend.
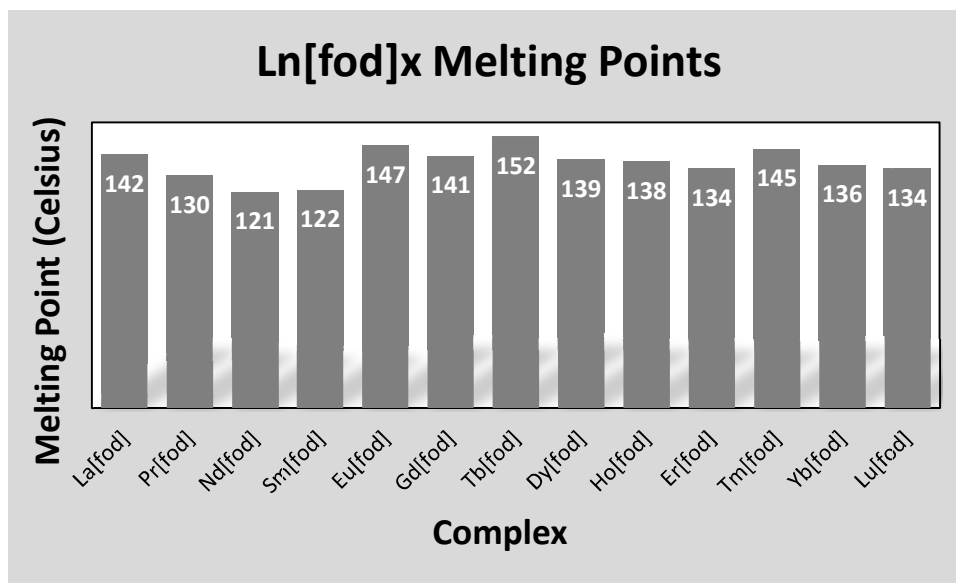
Figure 8-Distribution of Melting Points

iii.) Infrared (IR) Spectroscopy. FT-IR measurements were carried out the same as for the hfac ligand, and as before, only La, Gd, and Lu are shown in Table 14. Appendix 4 includes the expanded table for all the rare-earths analyzed. The IR peaks for $La[fod]_x$ and across the series in general were in good agreement with the data from Springer et al.[5]. Functional groups were assigned based on similarities to the hfac ligand complexes.

The major peaks are all identified and are listed in Table 14. Similar peaks were found for $NH_4[fod]$ which provides another standard for comparison. Table 14, as opposed to Table 6, presents a common IR peak value that may vary by ± 10 cm^{-1} for each peak.

There is excellent correlation can be found between the wavenumbers of the compounds from opposite ends of the lanthanide series, similar to the hfac ligand. However, it is not clear

where the distinction of metal-ligand wavenumbers can be resolved from the NH$_4$[fod] compound unlike with the hfac ligand. This created some ambiguity with the FT-IR as being the most reliable indicator of specific data; however, other data presented with the fod ligand helped to clearly identify the complexes.

Table 14- IR peaks (cm^{-1}) and functional group assignments for Ln[fod]$_x$ complexes

IR Peaks	NH4	La	Gd	Lu	Functional Assignment
3353 (br)	✓				O-H stretch
2974 (br)	✓	✓	✓	✓	C-H stretch
1624 (m, sh)	✓	✓	✓	✓	C=O stretch
1593 (w)	✓		✓	✓	C=C stretch
1509 (m, sh)	✓	✓	✓	✓	C-O stretch, C-H bend
1458 (m, sh)	✓	✓	✓	✓	C-H bend
1396 (w), 1368 (m, sh)	✓	✓	✓	✓	t-butyl groups
1344 (sh), 1276 (w), 1178 (m, sh), 1150 (sh)	✓	✓	✓	✓	C-F stretches
1220 (sh)		✓	✓	✓	C-F stretch
1117 (sh)		✓	✓	✓	C-H in plane bend
1103 (m, sh)	✓			✓	C-O stretch
1070 (m, sh)	✓	✓	✓	✓	C-O stretch
797 (w)	✓	✓	✓	✓	C-H out of plane bend
755 (w), 687 (w)	✓	✓	✓	✓	C-CF$_2$ stretches
741 (w)	✓	✓	✓	✓	C-CF$_3$ stretch

iv.) Nuclear Magnetic Resonance (NMR) Spectroscopy. NMR measurements were carried out on a Varian Inova 500 MHz instrument. The solvent used was 1,4-dioxane$_{(D-99.9\%)}$. Tables 15, 16, and 17 show the relative shifts of ^{13}C, ^{1}H, and ^{19}F NMR for the ligand (fod) by itself as well as the relative shifts for NH$_4$[fod], La[fod]$_x$, Gd[fod]$_x$, and Lu[fod]$_x$. Springer et al.[5] only show the

proton NMR, for which these peaks show a very close similarity in shift. For the ^{19}F NMR, Dolbier's text[15] was consulted for the assignment of peaks.

For the ^{13}C NMR, peaks (in ppm) are documented as follows: 93.4 corresponds to the α-carbon, 177.3 to the fluorine-winged β-carbon, and 203.8 to the t-butyl-winged β-carbon. The t-butyl carbon itself was shifted at 39.6 ppm as opposed to the methyl carbons at 26.4 ppm. Fluorinated carbons showed very low intensity signals that were difficult to assign beyond the general values listed in Table 15. The peak at 93.4 showed a triplet that is split most likely by the hydrogens instead of the fluorines. Both the β and t-butyl-winged carbons were singlets. There is no data listed for the other complexes due to issues with the C-probe. However, carbon-NMR was established more for completeness rather than for its relevance compared with the other NMR data.

Table 15-^{13}C-NMR (ppm) for fod ligand and fod complexes

	C-1	C-2	C-4	C-6	C-7	C-8	C-5	C-3
Hfod	26.4 (s)	39.6 (s)	93.4 (t)	~107	~109	~116-119	177.3 (s)	203.8 (s)
NH$_4$[fod], La[fod]$_x$, Gd[fod]$_x$, Lu[fod]$_x$	No data							

For the ^{1}H NMR, the ligand by itself shows a strong peak at 6.07 ppm corresponding to the hydrogens on the α-carbon. Compared to the hfac ligand, this peak is shifted more upfield due to the higher steric hindrance contributed especially by the t-butyl group. Another peak of less significance corresponding to the methyl hydrogen was found at 1.20 ppm. In the ammonium complex, ammonium hydrogens showed an additional quartet at 3.48 ppm. This shift is found somewhat between where amine groups (δ: 1.0-3.0) and ammonium cation shifts (δ: >

4.0) are found and can be correlated with how tightly the ammonium has coordinated to the ligand. This is pictorially represented in Figure 9.

Table 16- ^{1}H-NMR (ppm) for fod complexes

	C-1	C-4	NH$_4^+$
Hfod	1.20 (s)	6.07 (s)	
NH$_4$[fod]	1.23 (s)	6.07 (s)	3.48 (q)
La[fod]$_x$	1.09 (s)	5.95 (s)	
Gd[fod]$_x$	1.08 (s)	???	
Lu[fod]$_x$	1.1 (s)	6.06 (s)	

Another trend across the series is with respect to the α-hydrogen shift. La[fod]$_x$, for example, shows a peak at 5.95 ppm, Lu[fod]$_x$ at 6.06 ppm, and Gd[fod]$_x$ presumably between these two. One explanation for this might be in that the larger ion size of lanthanum contributes a higher shielding effect than lutetium, which contributes a shielding effect similar to ammonium. Another explanation that may run concurrently is that as lanthanum was observed to only have three ligands as opposed to four, that this might introduce less steric crowding in lanthanum's attempts to form a tighter coordination bond with the fod ligand. Hence, the oxygen atoms retain more of their electronic character and pull less at the α-hydrogen position. Conversely, lutetium with its smallest ionic radius and four ligands would bind the tightest, forcing the oxygen atoms to preserve their electronic character by pulling more at the α-hydrogen position. An important note to make is that this series is only observed substantially with respect to the α-hydrogen shift because this is the same location where the metal-ligand coordination takes place. This is also pictorially represented in Figure 10.

Table 17-^{19}F-NMR (ppm) for fod complexes

	C-6	C-7	C-8
Hfod	-127.6 (s)	-122.2 (q)	-81.4 (t)
NH$_4$[fod]	-126.9 (s)	-121.7 (q)	-80.6 (t)
La[fod]$_x$	-125.6	-121.7	-80.5
Gd[fod]$_x$	-126.4	-121.7	-80.5
Lu[fod]$_x$	-126.9	-120.3	-80.8

For the ^{19}F NMR, the ligand by itself showed strong peaks (in ppm) as follows: -127.6 corresponding to C-6, -122.2 corresponding to C-7, and -77.75 corresponding to C-8. Only the shift at C-8 bears resemblance to the shift in the hfac ligand due to the similar absence of steric bulk that is present around the interior of the ligand. The other fluorine shifts are moved significantly upfield. As for the ammonium and metal complexes, the reverse trend to the α-hydrogen shift H-NMR series is observed for its nearest fluorinated neighbor, C-6. Here, La[fod]$_x$ shows a peak at -125.6 ppm, Gd[fod]$_x$ at -126.4 ppm, Lu[fod]$_x$ at -126.9 ppm, and NH$_4$[fod] at -126.9 ppm. The reason for the reverse trend is that the C-6 fluorine atoms contribute more δ$^-$ to the stronger cationic charge of La (due to the weaker La-O bond present). In Lu, the stronger La-O bond does not require as much δ$^-$ contribution, so the fluorine atoms remain farther upfield. Electronically speaking, the order of 1 ppm translation across the series for C-6 fluorine shifts appears to be much less significant than the shifts due to the electronic interactions with the α-hydrogens. This should be expected due to the respective electronegativity differences of each site.
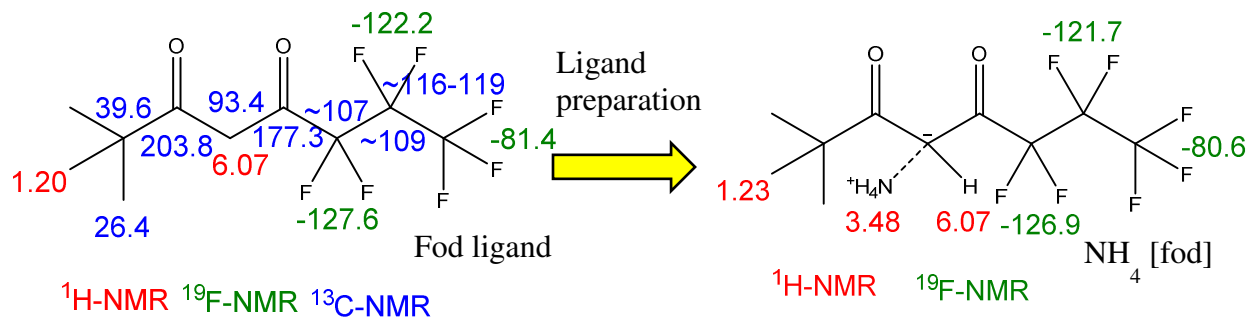
Figure 9 – NMR Shifts for Ammonium-Ligand Transformation Step

Fod ligand

^{1}H-NMR ^{19}F-NMR ^{13}C-NMR

NH$_4$ [fod]

^{1}H-NMR ^{19}F-NMR

Ligand preparation

-122.2
39.6 93.4 ~107 ~116-119
203.8 177.3 ~109
1.20 6.07 -81.4
26.4 -127.6

-121.7
1.23 3.48 6.07 -126.9 -80.6

La
-121.7
5.95
1.09 -80.5
-125.6

Gd
-121.7
???
1.08 -80.5
-126.4

Lu
-120.3
6.06
1.10 -80.8
-126.9

*Stronger metal-ligand coordination → α-hydrogen shifted further downfield

*Stronger metal-ligand coordination → C-6 fluorines shifted further upfield

Legend

^{1}H-NMR ^{19}F-NMR

Figure 10 – NMR Shifts for Metal-Ligand Coordination Complex

Finally, it should be noted that some information such as splitting patterns were unable to be deciphered from the NMR's involving the rare-earth complexes. In such cases, a splitting pattern is not listed in either Table 16 or 17. This is because many of the rare-earth metals carry with them inherently strong paramagnetic properties which interfere with the instrument to report precise shifts with high resolution. In all of the fluorine spectra analyzed, issues of line

broadening along with the inability to cancel noise contributed to a poor enough quality only to be able to assign the significant peaks. Figures 11 and 12 show two representative spectrums for the ^{1}H and ^{19}F NMR with this incidence.
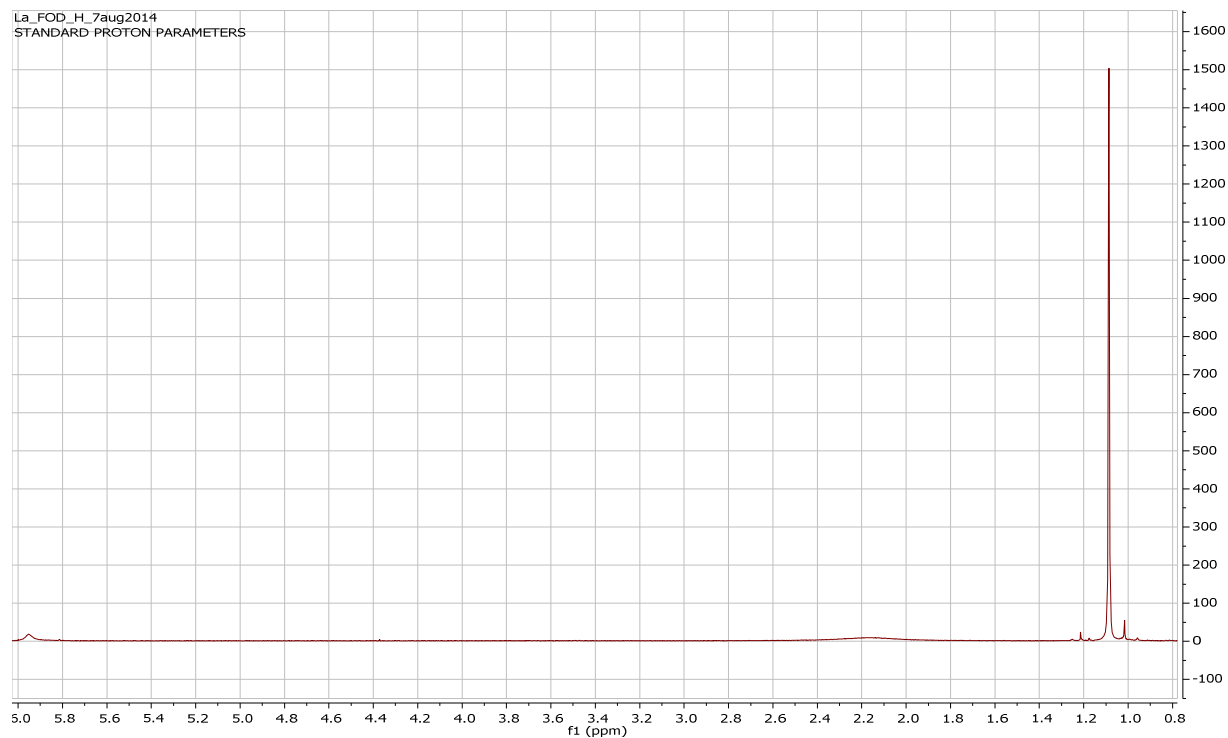
Figure 11- ^{1}H-NMR for La[fod]$_x$
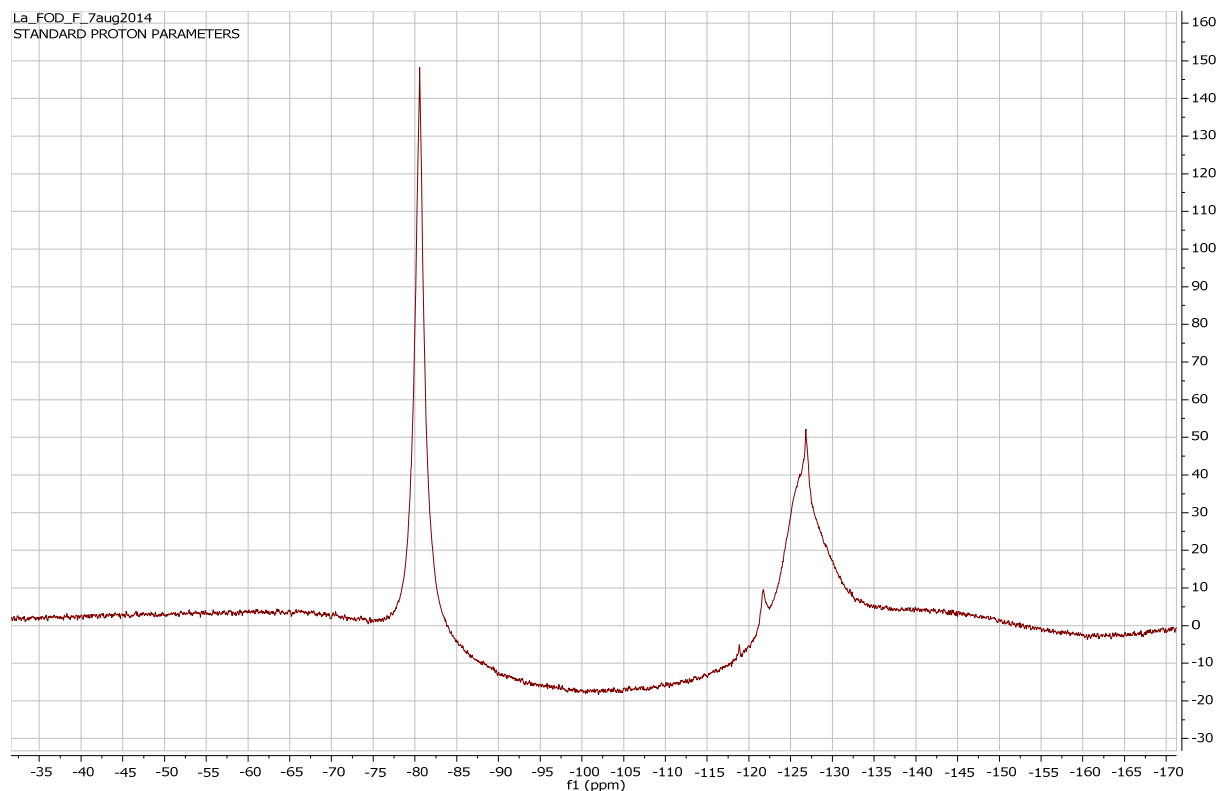
Figure 12- ^{19}F-NMR for La[fod]$_x$

IV.   Thermochromatographic Separations

A. *Ln[hfac]$_x$*

i.) Mass Fragmentation. In order to do thermochromatographic separations of the various rare-earth elements, one key preparation step is to have analyzed the mass fragmentation pattern for the ligand itself in order to see where any interference with the relative rare-earth ions may occur. This was carried out on NH$_4$[hfac].

Mass fragmentation was carried out on an Agilent6890GC/5973MSD. The carrier gas used was helium at a flow rate of 0.8 mL/min. The length of the column was 30 m. The injection inlet was heated to 250˚C to volatize the samples. The oven temperature was set to 45˚C, with a 2.00 min hold time. The oven was then heated at a rate of 5.0˚C/min to a set point 54˚C and held for 2.00 min, then increased to 65˚C at a ramp rate of 5˚C/min. Once at 65˚C, the ramp rate was

increased to 20°C/min and heated to 220°C. MS data was taken between 40-500 amu, but Figure 13 shows in a concise manner where the prevalent peaks for the hfac ligand take place. For example, at 208 amu is the mass fragment of the hfac molecule.

It can also be concluded that the most prevalent fragmentation takes place between the β and γ carbon atoms. This leaves two strong peaks at 69 and 139 amu. This same fragmentation can take place once or twice in the molecule. If it occurs twice, the 3-carbon interior fragment adds to 70 amu. The potential for overlap as well as the multiples of CF_3 fragments makes the 69 amu peak the strongest. Other moderate peaks at 91 and 119 amu are shown.

Ultimately, the important aspects of this figure show that the hfac ligand does not largely interfere with determining rare-earth ions with GC-MS. Rare-earth ion atomic weights range between 139-175 amu. Large interference would only occur with La[hfac]$_x$ at 139 amu. Therefore, the exception of La[hfac]$_x$ would potentially require more fragmentation of the ligand which would be possible with an ICP-MS instrument.
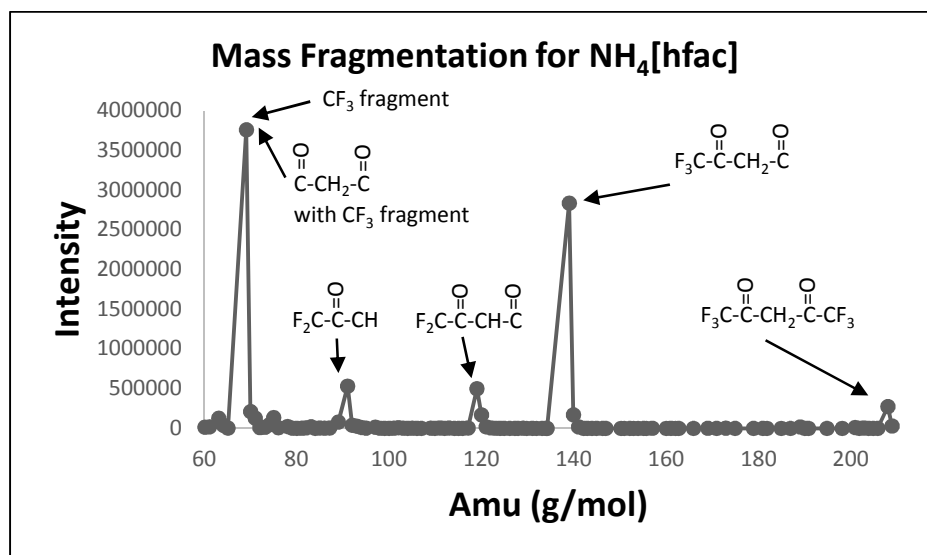
Figure 13-Mass Fragmentation for NH$_4$[hfac]

ii.) Separation of Sm, Dy, and Tm. Since there would be the least interference with Sm, Dy, and Tm, these elements were used as pilots for running initial separations. To keep consistency, the same method parameters were used as for the mass fragmentation above. Since the average mass of the rare-earth metal-ligand complex is greater than 1000 amu, its intact peak could not be seen due to the detector limit of 600 amu.

The chromatographic results from the separation are presented in Fig. 14. In the resulting chromatograph, the Sm complex is eluted at 3.6 min, the Dy complex is eluted at 4.2 min, and the Tm complex is eluted at 14.6 min. It should be noted that the peaks that are presented represent the response of the thermal conductivity detector (TCD) to the sample as it is eluted from the column and not the response from the mass spectrum detector.
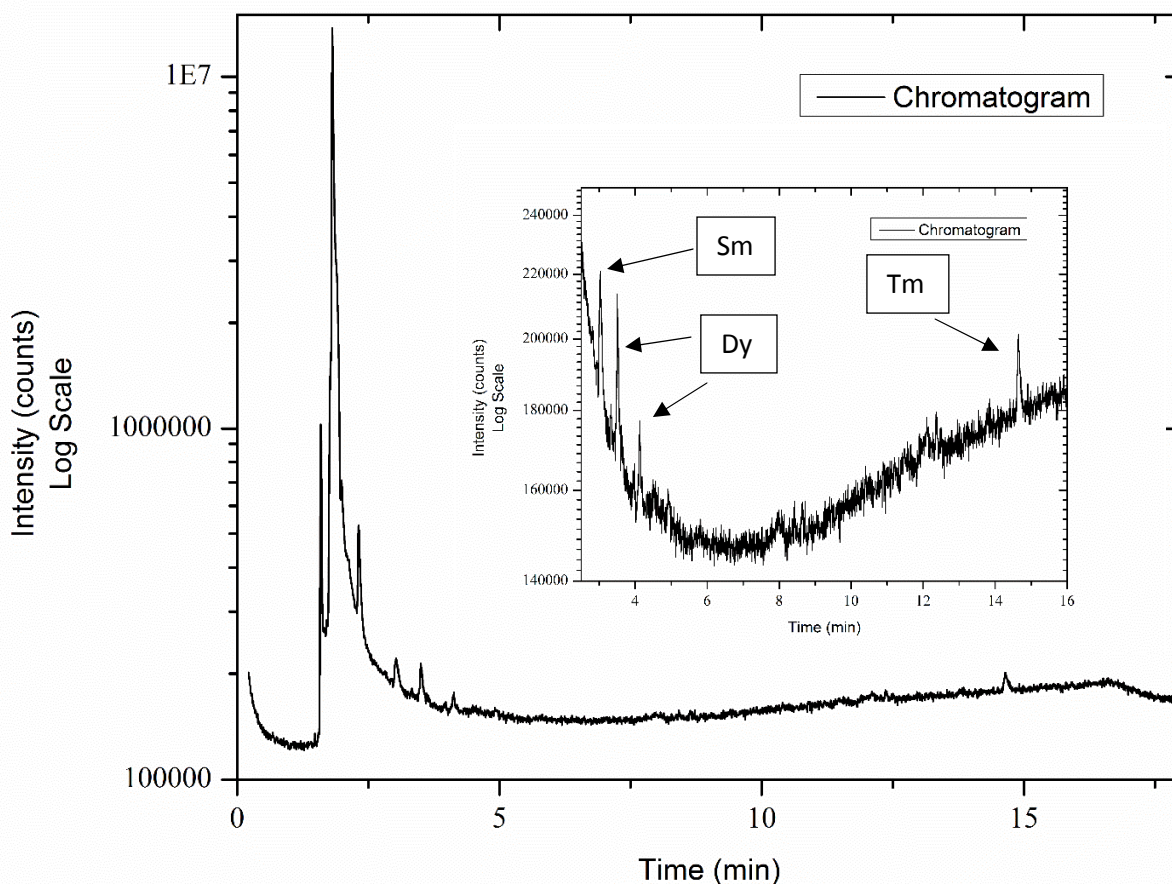
Figure 14- Chromatogram of ethyl ether containing 0.1 g/mL of Sm, Dy, and Tm Complex. Inserts highlight the point at which the compounds were eluted from the column

The chromatographic and mass spectra are shown in Figures 15-16. The separation profiles observed in Figs. 15-16 represent the response of the mass spectrum detector as a function of the number of scans taken. The total method time was approximately 14.8 min in length, and there were 2440 scans taken from the mass range of 1 to 500 amu. The response of the mass spectrum is similar to that of the FID detector and the resulting separation times are as follows: Sm is eluted at 3.2-3.5 min, Dy is eluted at 3.4-3.5 and 4.8-4.9 min, and Tm is eluted at 13.3-14.5 min. There is some overlap between the observed elution times of Sm and Dy.
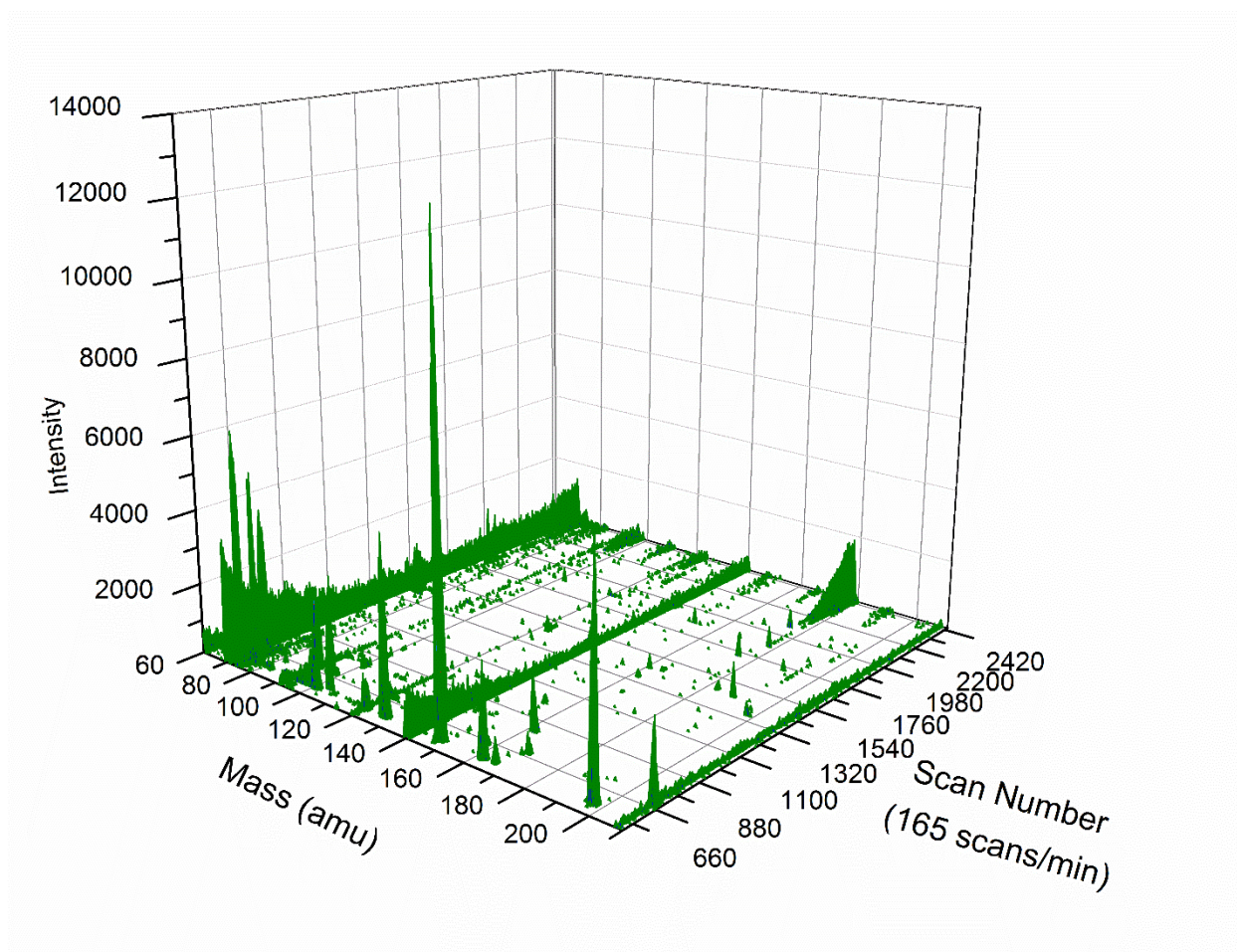
Figure 15-3D plot of the chromatographic separations. The large bands at 69, 78, 139, and 208 represent the ligand fragments
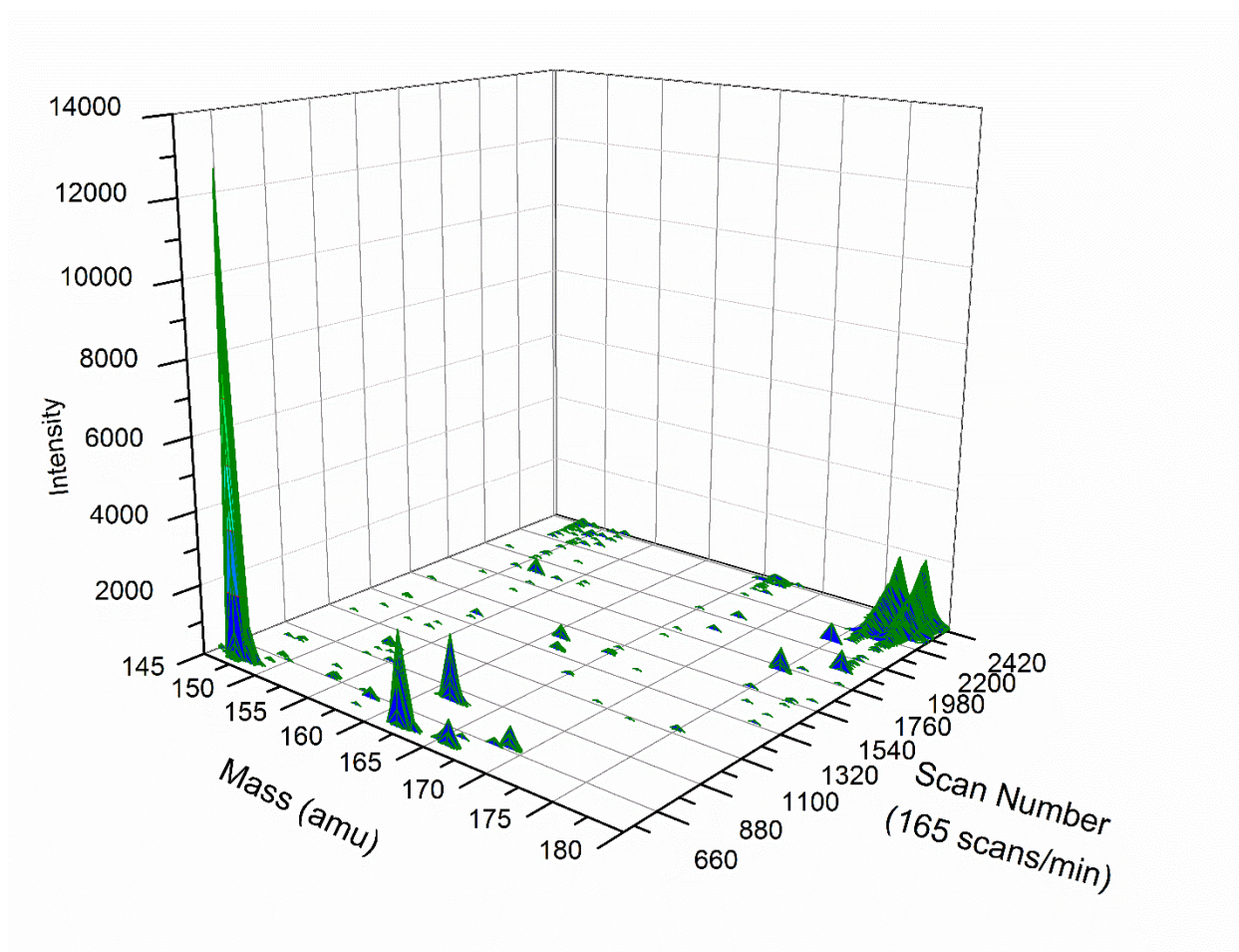
Figure 16- 3D plot of GC-MS data mass axis is restricted from 145 to 180 amu

B. *Ln[fod]*$_x$

i.) Mass Fragmentation. As with the hfac ligand, the fod ligand was run by itself through GC-MS to obtain the mass interference with relation to its own decomposition. Most of the parameters given below were the same ones used for the hfac ligand.

Mass fragmentation was carried out on an Agilent6890GC/5973MSD. The carrier gas used was helium at a flow rate of 0.8 mL/min. The length of the column was 30 m. The injection inlet was heated to 250 ˚C to volatize the samples. The oven temperature was set to 70˚C, with a

0.00 min hold time. The oven was then heated at a rate of 25.0°C/min to a set point 150°C and held for 5.00 min. MS data was taken between 60-210 amu, and Figure 17 shows where the prevalent peaks of interference for the fod ligand take place. The reference point for the whole ligand is 296.18 amu.

Since fod is an asymmetric ligand as opposed to hfac, Figure 17 shows a more complex fragmentation signature. As with hfac, fod has a prevalent fragmentation that takes place between the β and γ carbon atoms. However, because of its size and the resulting fragment instabilities, further fragmentation often takes place which explains the lower signal intensities for higher molecular weights that would correspond with one major fragmentation as in the hfac ligand. The only similarity to hfac is the strong peak at 69 amu. Oftentimes, a common trend is for the resulting fluorinated fragment to either decompose into fluorine gas or to oxidize which is shown, for example, between the range 130-170 amu.

As a result of this, it can be seen that the fod ligand has a larger spectrum of interference with determining rare-earth ions by GC-MS. Specifically, amu's of 151, 166, and 169 will be masked by fragmentation of fod. Rare-earth elements that would be difficult to determine with this ligand and method would be Eu and Tm. Therefore, these exceptions would potentially require more fragmentation of the ligand which would be possible with an ICP-MS instrument.
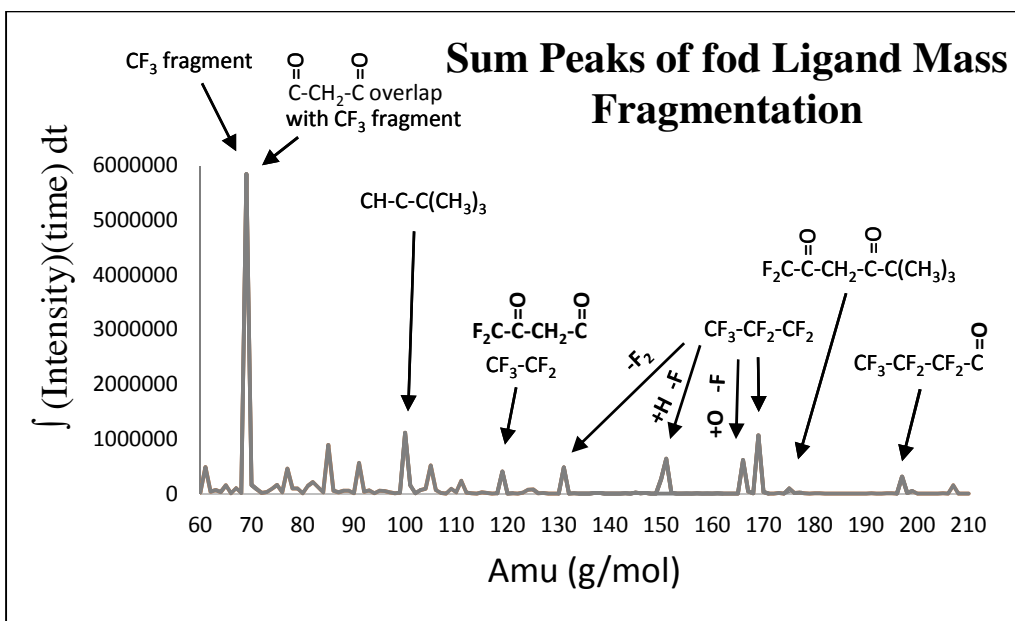
Figure 17- Mass Fragmentation for fod ligand

ii.) Separation of Nd, Sm, and Dy. Since Tm was observed to possess interference with the ligand, Nd served as a substitute. Therefore, there would be the least interference with Nd, Sm, and Dy, and these elements would be used to maintain as much consistency with the separation plot of the first ligand. However, the method parameters at this point were changed from the first ligand, although they are the same as used for the mass fragmentation above. Once again, since the average mass of the rare-earth metal-ligand complex is greater than 1000 amu, its intact peak could not be seen due to the detector limit of 600 amu.

The chromatographic results from the separation are presented in Fig. 18. In the resulting chromatograph, the Nd, Sm, and Dy complexes are all eluted at around 2.5-2.6 min. However, from the unadjusted intensities and no mass spectra, the differentiated peaks for each rare-earth complex cannot be told apart.

One other point to note is that the solubility differences are substantial between the complexes with the hfac ligand versus the fod ligand. It was found on individual runs that about 5 mg/mL could be dissolved in solution for the Sm and Dy complexes while Nd complexes had much poorer solubility, dissolving only about 0.125 mg/mL in ethyl ether. Their combined concentration by weight is listed in Figure 18; however, it should be noted that this is an average and not an equally weighted solution.
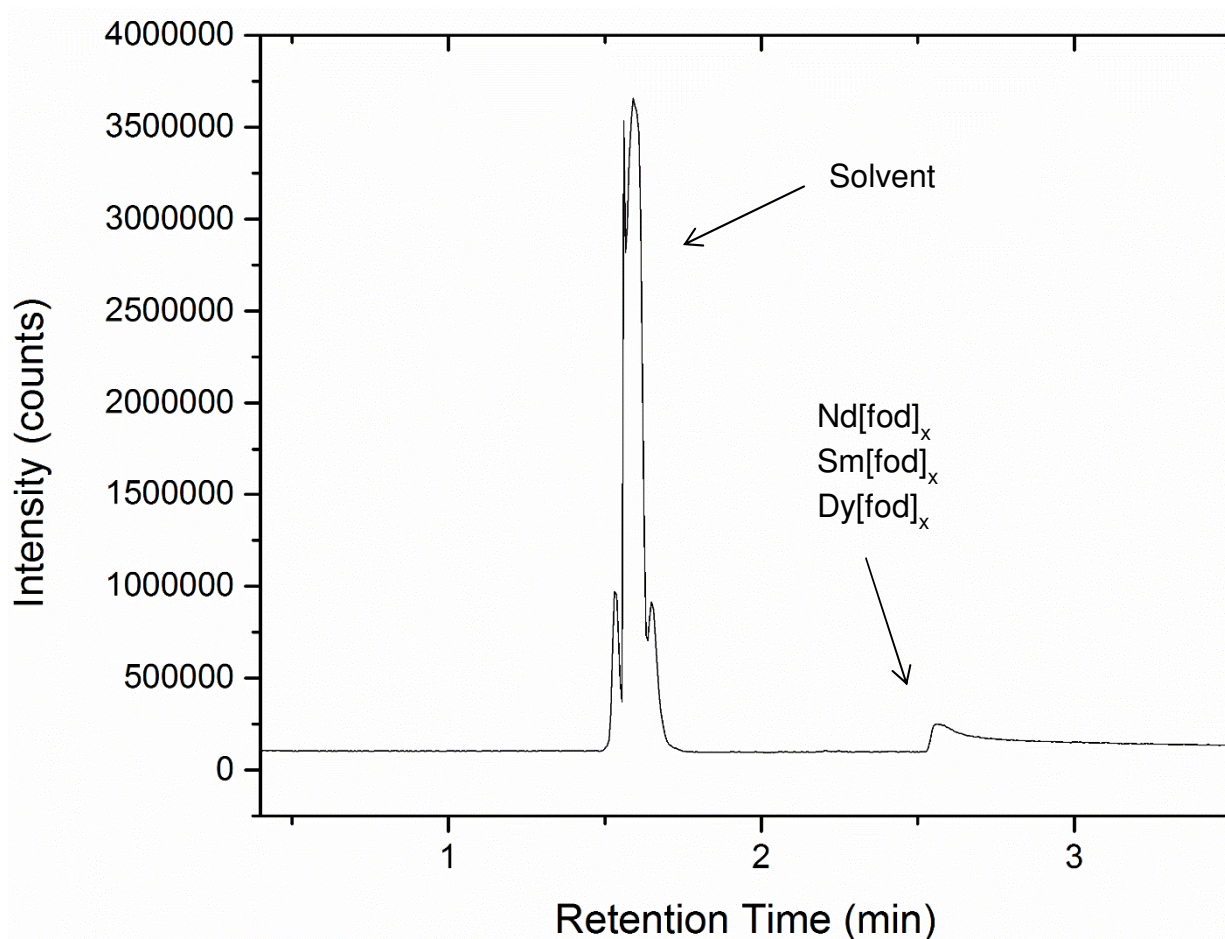
Figure 18- Chromatogram of ethyl ether containing 3.373 mg/mL of Nd, Sm, and Dy Complex.

The chromatographic and mass spectra are shown in Figure 19. The separation profiles observed in Fig. 19 represent the response of the mass spectrum detector as a function of the number of scans taken. The total method time was approximately 8.0 min in length, and there

were 1320 scans taken from the mass range of 1 to 500 amu. The response of the mass spectrum

is similar to that of the FID detector and the resulting separation times are as follows: Nd is

eluted at 2.4-2.9 min, Sm is eluted at 2.4-2.8 min, and Dy is eluted at 2.4-2.6 min. Overlap

dominates the observed elution times for all three rare-earth complexes**.**
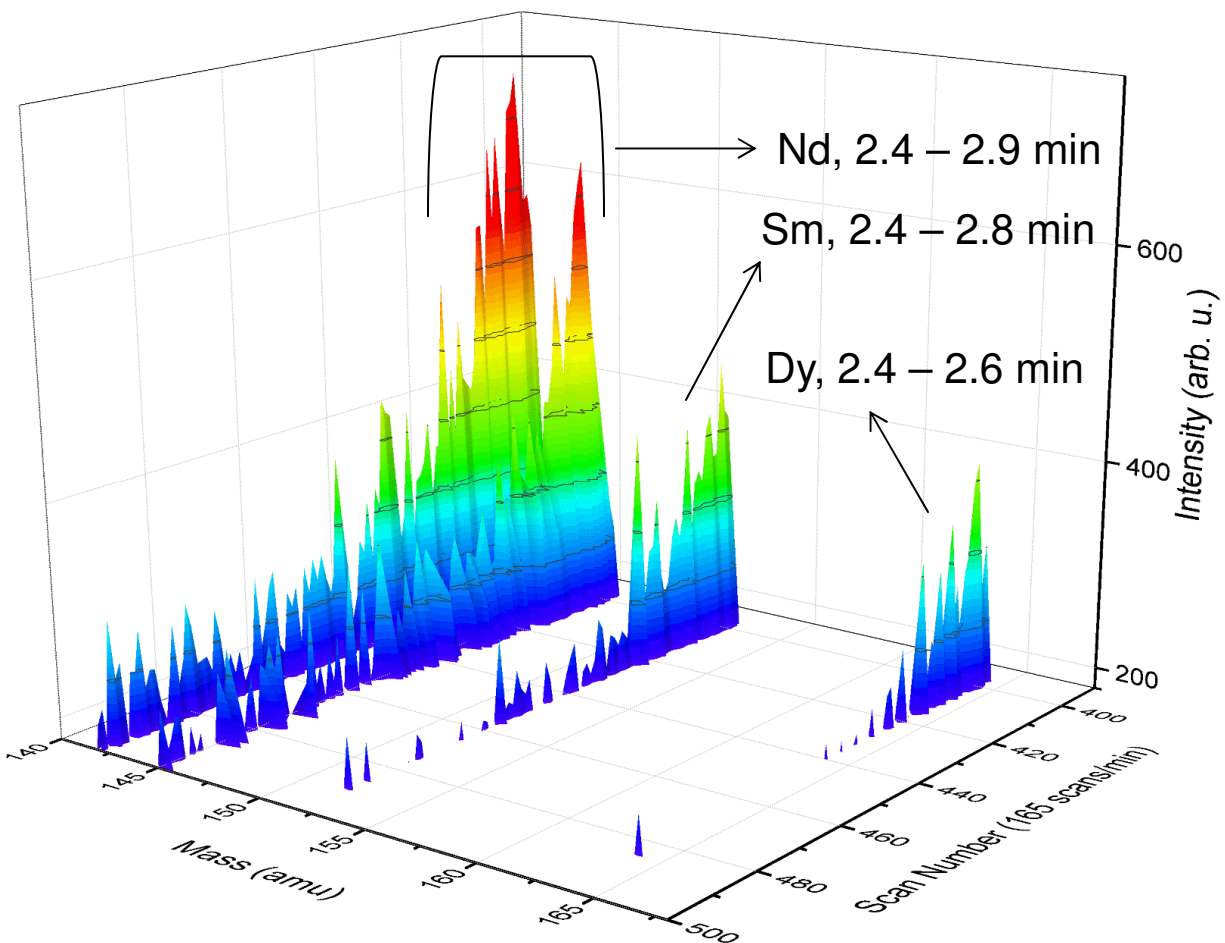
Figure 19- 3D plot of the chromatographic separations. Bands represent Nd (142 & 146), Sm (152), and Dy (165). The mass axis is restricted from 140 to 170 amu.

V.   Conclusions

Based on the analysis performed, the compounds synthesized were the desired $Ln[hfac]_x$

and $Ln[fod]_x$ compounds. The IR and NMR data showed that both the hfac and fod ligands were

forming M-O bonds with the central lanthanide atom. New melting point data was obtained for

several lanthanides including $Gd[hfac]_x \cdot XH_2O$ and $Lu[hfac]_x \cdot XH_2O$, and melting point data for several others including $La[hfac]_x \cdot XH_2O$ were confirmed. It was also found that melting point data for $Ln[fod]_x$ across the series bears no resemblance to the clear Shannon-Prewitt radii relationship seen in $Ln[hfac]_x$ complexes. Computational and elemental analysis (and in one case SC-XRD) strongly pointed to $La(hfac)_x \cdot XH_2O$ existing primarily as $NH_3^+(La[hfac]_4^-)$, Gd existing as $NH_3^+(Gd[hfac]_4^-)$, and Lu existing as $NH_3^+(Lu[hfac]_4^-)$ with a decrease in hydration across the series. However, NMR data suggested the presence of other minor complexes too. For the fod ligand, the same set of analyses suggested both the three and four ligand complex. For example, $La[fod]_x$ existed as $La[fod]_3$ while Gd existed as $NH_3^+(Gd[fod]_4^-)$.

In the early stages of thermochromatographic separations with the hfac ligand, mass fragmentation suggested that there would be little interference from the ligand when identifying GC separation peaks for rare-earths, excluding La. In contrast, the mass fragmentation for the fod ligand suggested that there would be interference for europium and thulium. Finally, separation of Sm, Dy, and Tm complexes (hfac) proved to be an initial success for finding a rapid method of rare-earth element separation. For the fod ligand, rapid separations proved to be more difficult to achieve both in synthesis preparation time and in resolution of rare-earth peaks that overlap. Future work for this project will involve obtaining good SC-XRD data to confirm the coordination number and crystal structure of the rest of these compounds. Additionally, an enhanced methodology will be developed for finding good separation parameters for all 14 lanthanides (not Pm) with GC-MS.

VI. References

1. Eisentraut, K.J. and Sievers, R.E. Volatile rare-earth chelates. *Journal of the American Chemical Society*, **1965**, *87* (22), 5254-5256.

2. Binnemans, K. Rare-earth beta-diketonates. In *Handbook on the Physics and Chemistry of Rare Earths*, K.A. Gschneidner, J-C. Bünzli, and V.K. Pecharsky, Eds. Elsevier: **2005**, Vol. 35, 107-272.

3. Bauer, H., Blanc, J., and Ross, D. L. Octacoordinate chelates of lanthanides. Two series of compounds. *Journal of the American Chemical Society*, **1964**, *86* (23), 5125-5131.

4. Berg E.W. and Acosta, J.J.C. Fractional sublimation of the -diketone chelates of the lanthanide and related elements. *Analytica Chimica Acta*, **1968**, *40*, 101-113.

5. Springer, C.S., Meek, D.W., and Sievers, R.E. *Inorganic Chemistry*, **1967,** *6*, 1105-1110.

6. Halverson, F., Brinen, J.S., and Leto, J.R. *The Journal of Chemical Physics*, **1964,** *40*, 2790-2792.

7. Ahmed, Z. and Iftikhar, K., *Inorganica Chimica Acta*, **2012,** *392*, 165-176.

8. Hanson, D.E., Garrison, J.R., and Hall, H.L. Assessing thermochromatography as a separation method for nuclear forensics: current capability vis-a-vis forensic requirements. *Journal of Radioanalytical and Nuclear Chemistry*, **2011**, *289* (1), 213-223.

9. Sievers, R.E., Eisentraut, K.J., and Springer, Jr., C.H. Volatile rare-earth chelates of -diketones." In *Lanthannide/Actinide Chemistry* by Fields, P. et al., Advances in Chemistry, ACS: Washington D.C., **1967**.

10. Shannon, R.D. Revised effective ionic radii and systematic studies of interatomic distances in halides and chalcogenides. *Acta Cryst.*, **1976**, A**32**, 751-767.

11. Atwood, David A. *The Rare-Earth Elements: Fundamentals and Applications*. John Wiley & Sons, **2013**.

12. Richardson M.F., Wagner, W.F., & Sands, D.E. Rare-earth trishexafluoroacetylacetonates and related compounds. *Journal of Inorganic & Nuclear Chemistry*, **1968**, *30* (5), 1275-1289.

13. Condorelli, G.G., Gennaro, S., and Fragalà, I. L. *Chemical Vapor Deposition*, **2001,** *7*, 151-156.

14. Aygen, S. and van Eldik, R. A spectroscopic and mechanistic study of the enolization and diol formation of hexafluoroacetylacetone in the presence of water and alcohol. *Chemische Berichte*, **1989**, 315-320.

15.   Dolbier, Jr., William R. *Guide to Fluorine NMR for Organic Chemists.* John Wiley & Sons Inc., Hoboken, NJ. **2009**.

VII. Appendices

Appendix 1- Other Rare-Earth [hfac] Elemental Analysis Tables

Pr: 65.94-68.34% yield (45.78%)			
Element	Theory	Found	% Error
C	24.5	24.52	0%
H	1.44	1.49	3%
N	2.86	3.095	8%
F	46.51	46.11	1%

Nd: 74.53-77.24% yield (44.48%)			
Element	Theory	Found	% Error
C	24.46	24.495	0%
H	1.76	1.81	2%
N	4.07	4.185	3%
F	46.42	45.17	3%

Sm: 35.04-36.31% yield (20.96%)			
Element	Theory	Found	% Error
C	24.37	24.3	0%
H	1.75	1.87	6%
N	4.06	4.06	0%
F	45.8	----	----

Eu: 61.99-64.23% yield (55.47%)			
Element	Theory	Found	% Error
C	23.4	24.605	5%
H	1.35	1.58	14%
N	2.43	2.525	4%
F	44.42	44.47	0%

Tb: 64.41-66.72% yield (30.19%)			
Element	Theory	Found	% Error
C	24.35	24.52	1%
H	2	2.27	12%
N	4.42	4.515	2%
F	46.22	46.19	0%

Dy: 72.47-75.06% yield (42.67%)			
Element	Theory	Found	% Error
C	23.71	24.45	3%
H	1.93	2.08	7%
N	3.95	3.865	2%
F	45	46.1	2%

Ho: 64.87-67.18% yield (63.11%)			
Element	Theory	Found	% Error
C	23.73	23.72	0%
H	0.87	0.86	1%
N	1.63	1.65	1%
F	45.05	----	----

Er: 50.78-52.59% yield (35.53%)			
Element	Theory	Found	% Error
C	24.04	24.27	1%
H	1.41	1.66	15%
N	2.8	3.3	15%
F	45.64	45.73	0%

Tm: 57.15-59.18% yield (52.02%)			
Element	Theory	Found	% Error
C	23.42	24.18	3%
H	1.18	1.18	0%
N	2.43	2.5	3%
F	44.46	----	----

Yb: 66.12-68.45% yield (62.72%)			
Element	Theory	Found	% Error
C	23.42	23.73	1%
H	0.97	0.95	2%
N	1.68	1.69	1%
F	44.45	----	----

Appendix 2- Other Rare-Earth [hfac] FT-IR Spectroscopic Data

Pr	Nd	Sm	Eu	Tb	Dy	Ho	Er	Tm	Yb	Functional Assignment
743	743	744	743	738	738	744	745	744	745	C-CF$_3$ stretch
805	805	805	804	821	800	804	803	804	802	C-H out of plane bend
1135	1135	1130	1132	1132	1123	1132	1134	1132	1120	C-H in-plane bend
1179	1177	1179	1147	1147	1177	1175	1175	1177	1178	C-F stretch
1198	1198	1194	1203	1202	1196	1203	1201	1203	1200	C-F stretch
1252	1253	1252	1250	1251	1253	1251	1254	1251	1254	C-F stretch
1462	1462	1440	1501	1403	1459	1477	1474	1473	1478	C-H bend, [hfac]-metal coordination
1538	1537	1538	1536	1537	1535	1537	1536	1537	1537	C-O stretch, C-H bend, [hfac]-metal coordination
1562	1563	1563	1564	1564	1564	1565	1564	1564	1565	C=C stretch, [hfac]-metal coordination
1643	1643	1644	1644	1645	1645	1647	1646	1649	1647	C-O stretch, [hfac]-metal coordination
3218	3215	3184	3148	3148	3211	3238	3219	3149	3149	O-H stretch

Appendix 3- Other Rare-Earth [fod] Elemental Analysis Tables

Pr: 57.89-59.97% yield. (58.91%)			
Element	Theory	Found	% Error
C	34.98	35.645	2%
H	3.38	3.46	2%
N	1.02	1.085	6%
F	38.72	39.46	2%

Nd: 57.89-59.97% yield. (58.91%)			
Element	Theory	Found	% Error
C	34.89	34.865	0%
H	3.37	3.335	1%
N	1.02	1.02	0%
F	38.63	38.22	1%

Sm: 57.89-59.97% yield. (58.91%)			
Element	Theory	Found	% Error
C	34.35	33.415	3%
H	3.32	3.22	3%
N	0.67	0.63	6%
F	38.03	36.81	3%

Eu: 57.89-59.97% yield. (58.91%)			
Element	Theory	Found	% Error
C	34.7	35.165	1%
H	3.35	3.515	5%
N	1.01	1.06	5%
F	38.42	38.02	1%

Tb: 57.89-59.97% yield. (58.91%)			
Element	Theory	Found	% Error
C	34.48	34.95	1%
H	3.38	3.39	0%
N	1.16	1.14	2%
F	38.54	38.5	0%

Dy: 57.89-59.97% yield. (58.91%)			
Element	Theory	Found	% Error
C	34.43	34.67	1%
H	3.32	3.28	1%
N	1	1.025	2%
F	38.13	38.09	0%

Ho: 57.89-59.97% yield. (58.91%)			
Element	Theory	Found	% Error
C	34.37	34.765	1%
H	3.32	3.27	2%
N	1	1.02	2%
F	38.06	38.25	0%

Er: 57.89-59.97% yield. (58.91%)			
Element	Theory	Found	% Error
C	34.32	33.55	2%
H	3.31	3.245	2%
N	1	1.09	8%
F	38	36.09	5%

Tm: 57.89-59.97% yield. (58.91%)			
Element	Theory	Found	% Error
C	34.28	34.595	1%
H	3.31	3.225	3%
N	1	0.98	2%
F	37.95	38.12	0%

Yb: 57.89-59.97% yield. (58.91%)			
Element	Theory	Found	% Error
C	34.27	34.245	0%
H	3.34	3.185	5%
N	0.8	0.795	1%
F	36.86	37.72	2%

Appendix 4- Other Rare-Earth [fod] FT-IR Spectroscopic Data

IR Peaks	Pr	Nd	Sm	Eu	Tb	Dy	Ho	Er	Tm	Yb	Functional Assignment
3353 (br)		✓									O-H stretch
2974 (br)	✓	✓	✓	✓	✓	✓	✓	✓	✓	✓	C-H stretch
1624 (m, sh)	✓	✓	✓	✓	✓	✓	✓	✓	✓	✓	C=O stretch
1593 (w)		✓	✓		✓	✓	✓	✓	✓	✓	C=C stretch
1509 (m, sh)								✓	✓	✓	C-O stretch, C-H bend
1458 (m, sh)	✓	✓	✓	✓	✓	✓	✓	✓	✓	✓	C-H bend
1396 (w), 1368 (m, sh)	✓	✓	✓	✓	✓	✓	✓	✓	✓	✓	t-butyl groups
1344 (sh), 1276 (w), 1178 (m, sh), 1150 (sh)								✓	✓		C-F stretches
1220 (sh)	✓	✓	✓	✓	✓	✓	✓	✓	✓	✓	C-F stretch
1117 (sh)	✓	✓	✓	✓	✓	✓	✓	✓	✓	✓	C-H in plane bend
1103 (m, sh)	✓		✓	✓	✓	✓	✓	✓	✓	✓	C-O stretch
1070 (m, sh)	✓	✓	✓	✓	✓	✓	✓	✓	✓	✓	C-O stretch
797 (w)	✓	✓	✓	✓	✓	✓	✓	✓	✓	✓	C-H out of plane bend
755 (w), 687 (w)	✓	✓	✓	✓	✓	✓	✓	✓	✓	✓	C-CF$_2$ stretches
741 (w)	✓	✓	✓	✓	✓	✓	✓	✓	✓	✓	C-CF$_3$ stretch